Cell Metabolism
Article

Immunoresponsive Gene 1 Augments Bactericidal Activity of Macrophage-Lineage Cells by Regulating β-Oxidation-Dependent Mitochondrial ROS Production

Christopher J. Hall,[1] Rachel H. Boyle,[1] Jonathan W. Astin,[1] Maria Vega Flores,[1] Stefan H. Oehlers,[1] Leslie E. Sanderson,[1] Felix Ellett,[2] Graham J. Lieschke,[2] Kathryn E. Crosier,[1] and Philip S. Crosier[1,*]
[1]Department of Molecular Medicine and Pathology, School of Medical Sciences, The University of Auckland, Auckland 1023, New Zealand
[2]Australian Regenerative Medicine Institute, Monash University, Wellington Road, Clayton, VIC 3800, Australia
*Correspondence: ps.crosier@auckland.ac.nz
http://dx.doi.org/10.1016/j.cmet.2013.06.018

SUMMARY

Evidence suggests the bactericidal activity of mitochondria-derived reactive oxygen species (mROS) directly contributes to killing phagocytozed bacteria. Infection-responsive components that regulate this process remain incompletely understood. We describe a role for the mitochondria-localizing enzyme encoded by *Immunoresponsive gene 1* (*IRG1*) during the utilization of fatty acids as a fuel for oxidative phosphorylation (OXPHOS) and associated mROS production. In a zebrafish infection model, infection-responsive expression of zebrafish *irg1* is specific to macrophage-lineage cells and is regulated cooperatively by glucocorticoid and JAK/STAT signaling pathways. Irg1-depleted macrophage-lineage cells are impaired in their ability to utilize fatty acids as an energy substrate for OXPHOS-derived mROS production resulting in defective bactericidal activity. Additionally, the requirement for fatty acid β-oxidation during infection-responsive mROS production and bactericidal activity toward intracellular bacteria is conserved in murine macrophages. These results reveal IRG1 as a key component of the immunometabolism axis, connecting infection, cellular metabolism, and macrophage effector function.

INTRODUCTION

The emerging field of immunometabolism has its basis in the observation that inflammation is a "hallmark" of many chronic metabolic disorders (Mathis and Shoelson, 2011). Central to this link between the immune and metabolic systems is the mitochondrion. In addition to roles during cellular metabolism and apoptosis, mitochondria are becoming recognized as central players in the orchestration of inflammatory pathways and immune cell function (Manfredi and Rovere-Querini, 2010; West et al., 2011b). Studies have linked the production of mitochondrial reactive oxygen species (mROS), a byproduct of oxidative phosphorylation (OXPHOS), and macrophage-mediated bactericidal activity (Sonoda et al., 2007; West et al., 2011a). In an active process, mitochondria are recruited to phagosomes containing phagocytozed bacteria to deliver OXPHOS-generated bactericidal ROS (West et al., 2011a). How mitochondrial metabolism influences immune cell function, and what signaling cascades help drive cell-intrinsic metabolic modes in immune cells, is incompletely understood and an area of intense interest.

Identified as an LPS-inducible gene within macrophages, *immunoresponsive gene 1* (*IRG1*) is highly conserved in vertebrates, suggesting an important role during the immune response (Lee et al., 1995). IRG1 is the mammalian ortholog of bacterial 2-methylcitrate dehydratase (encoded by the *prpD* gene), an enzyme that functions during catabolism of the short-chain fatty acid propionate (propanoate/propionic acid). In light of this, and given that IRG1 localizes to the mitochondria, we reasoned that IRG1 may represent a key component linking immunological and metabolic processes (Degrandi et al., 2009).

The zebrafish is a well-established model in which to study innate immune cell function. By 2 days postfertilization (dpf), zebrafish embryos are populated with macrophage lineages that are functionally similar to those in humans. Live imaging macrophage-lineage-specific transgenic zebrafish has enabled unique insights into their innate immune cell function (Ellett et al., 2011; Roca and Ramakrishnan, 2013). More recently, live imaging of fluorescent fatty acid analogs within transparent zebrafish embryos and larvae has given researchers the ability to directly observe their cellular metabolism, resulting in new mechanistic insights into lipid metabolism (Carten et al., 2011; Semova et al., 2012). Most of our understanding regarding metabolic modes of immune cells has been gleaned from in vitro cell culture-based studies. The live imaging potential of the genetically tractable zebrafish system provides a unique opportunity to directly observe how the metabolic mode of immune cells influences their activity in the context of an intact cellular environment.

Exploiting the zebrafish system, we have examined the functional role of the zebrafish ortholog of IRG1 (Irg1) during the innate immune cell response to bacterial infection. We show that zebrafish *irg1* is rapidly expressed within macrophage-lineage cells in response to bacterial infection. We further reveal that infection-responsive expression of *irg1* is dependent on the "primary response" transcription factor C/ebpβ and the cooperative activity of the glucocorticoid receptor (GR) and JAK/STAT signaling pathways. Mitochondria of Irg1-depleted

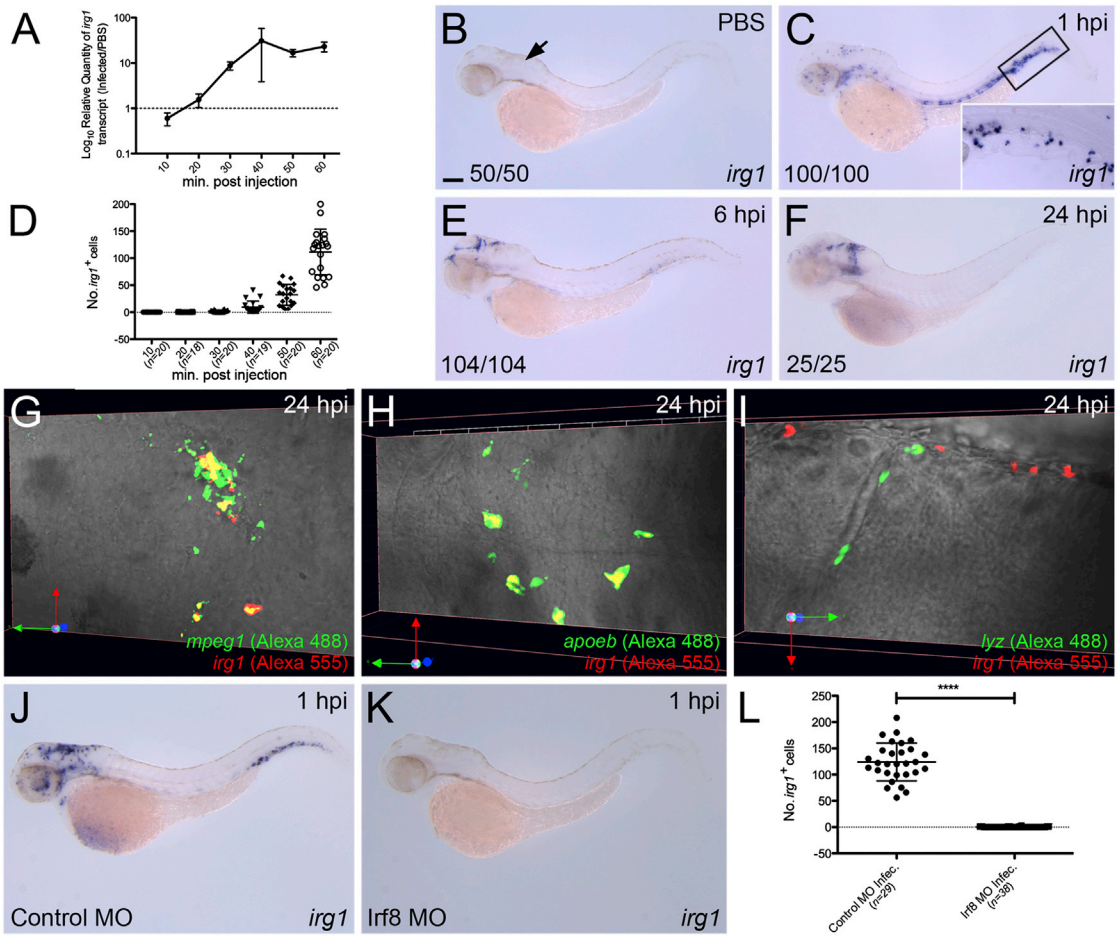

Figure 1. Macrophage-Lineage Cells Express *irg1* in Response to Infection

(A) Temporal QPCR analysis of *irg1* expression within infected larvae (relative to PBS-injected controls) throughout first hour of infection, n = 3 biological replicates (mean ± SD).

(B and C) Expression of *irg1* within PBS-injected control and infected larvae at 1 hpi, respectively. Arrow marks hindbrain ventricle injection site. Inset, magnified view of boxed region of similarly treated larva (10× objective).

(D) Quantification of *irg1*$^+$ cells within individual infected larvae at 10, 20, 30, 40, 50, and 60 mpi (mean ± SD).

(E and F) Expression of *irg1* within infected larvae at 6 and 24 hpi, respectively.

(G–I) Dual expression analysis of *irg1* and *mpeg1* (G), *apoeb* (H), and *lyz* (I) within the midbrain/hindbrain region of infected larvae at 24 hpi.

(J and K) Expression of *irg1* within infected control MO-injected and Irf8-depleted larvae, respectively, at 1 hpi.

(L) Quantification of *irg1*$^+$ cells within individual infected larvae as shown in (J) and (K) (mean ± SD). All views anterior to left. Numbers represent frequency of larvae with displayed phenotype. Scale bar, 100 μm in (B). ****$p < 0.0001$. See also Figure S1.

macrophage-lineage cells are deficient in their ability to utilize fatty acids as an energy substrate for mitochondrial OXPHOS and mROS production, resulting in decreased bactericidal activity. We also reveal a conserved dependence on fatty acid β-oxidation for mROS production and bactericidal activity within stimulated murine macrophages. We propose that IRG1 functions within the mitochondria of activated macrophage-lineage cells to enhance the utilization of "energetically efficient" fatty acid β-oxidation. The resulting increase in OXPHOS amplifies mROS production that helps augment macrophage bactericidal activity toward intracellular bacteria. These results reveal IRG1 as a key component of the immunometabolism axis connecting infection, mitochondrial metabolism, and macrophage effector function.

RESULTS

Zebrafish *irg1* Is Expressed within Macrophage-Lineage Cells in Response to Infection

We first identified the zebrafish ortholog of human *IRG1* as a gene upregulated in response to *Salmonella enterica* serovar Typhimurium (hereafter referred to as *Salmonella*) infection using the GeneChip Zebrafish Genome Array (Affymetrix) (data not shown). Quantitative (q)PCR analysis of *irg1* expression in response to *Salmonella* (600 colony-forming units [cfu] injected into the hindbrain ventricle at 52 hpf) revealed elevated expression as early as 30 min postinjection (mpi), when compared with PBS control-injected larvae (Figure 1A). Of note, uninjected and PBS control-injected larvae demonstrated no

irg1 expression (Figure 1B). Throughout the remainder of this study, unless otherwise stated, an infection dose of 600 cfu of *Salmonella* was microinjected into the hindbrain ventricle at 52 hpf. From 40 mpi, *irg1*-expressing cells were increasingly detected throughout the trunk and tail vasculature and within the midbrain and hindbrain of infected larvae (Figures 1C and 1D). From 6 hr postinjection (hpi), expression became restricted to the midbrain and hindbrain (Figures 1E and 1F). Expression analysis revealed that *irg1*-expressing cells were also positive for the macrophage-lineage marker *mpeg1* and microglial marker *apolipoprotein Eb* (*apoeb*) but not the neutrophil-specific marker *lysozyme C* (*lyz*), consistent with a macrophage-lineage phenotype (Figures 1G–1I). In zebrafish larvae, microglia differentiate from macrophages that have invaded the developing brain from ~60 hpf (Herbomel et al., 2001). In light of this, throughout the remainder of this study we refer to *irg1*- and *mpeg1*-expressing cells within the midbrain and hindbrain region as macrophage-lineage cells. Irf8 promotes macrophage lineage commitment at the expense of neutrophil development such that Irf8-deficient larvae are depleted of macrophage-lineage cells and possess an expanded neutrophil compartment (Li et al., 2011). In support of *irg1* expression being restricted to macrophage-lineage cells, infection-responsive *irg1* expression was completely abolished within morpholino oligonucleotide (MO)-mediated Irf8-depleted larvae (Figures 1J–1L and see Figures S1A–S1E online). In addition to live bacterial challenge, injection of Toll-like receptor (TLR) ligands, in particular lipopolysaccharide (LPS) and flagellin, stimulated *irg1* expression (Figures S1F and S1G). Consistent with previous studies, infection-responsive expression of *irg1* was not dependent on the TLR adaptor MyD88 (Kawai et al., 2001; van der Vaart et al., 2013) (Figures S1H–S1K).

These results demonstrate that *irg1* expression is rapidly induced within macrophage-lineage cells in response to live bacterial challenge and TLR agonist stimulation.

Expression of *irg1* Is Dependent upon the Infection-Responsive Primary Response Gene *cebpβ*

Due to the rapid kinetics of *irg1* expression in response to infection, we assessed whether expression was dependent on de novo protein synthesis. Larvae treated with cycloheximide (CHX) demonstrated an almost complete inhibition of infection-responsive *irg1* expression (Figures 2A–2C). This result confirmed that *irg1* is a "secondary response" gene within activated macrophage-lineage cells that likely relies upon infection-responsive ("primary response") regulators for transcriptional activation. Analysis of the promoter region of *irg1* revealed a number of consensus binding motifs for the transcription factor C/EBPβ (Figure S2A). C/EBPβ is a known transcriptional regulator of the acute phase response, where it functions as a primary response gene (Matsuno et al., 1996). Similar to *irg1*, *cebpβ* was expressed in cells throughout the trunk vasculature following infection (Figure 2D). Of note, constitutive expression of *cebpβ* was observed within the developing liver and intestine of PBS-injected control larvae (Figure 2D). However, unlike *irg1*, infection-responsive *cebpβ* expression was maintained in the presence of CHX, confirming its classification as a primary response gene within activated macrophage-lineage cells (Figure 2D). Of interest, CHX treatment of infected and PBS-injected larvae resulted in elevated expression of *cebpβ* when compared with DMSO-treated larvae (Figure 2D), raising the possibility that expression of *cebpβ* is, in part, controlled via a transcriptional repressor. Consistent with this result, primary response genes have been shown to be uniquely associated with corepressor complexes to prevent signal-independent missexpression (Hargreaves et al., 2009). We anticipate this is a mechanism to suppress infection-independent missexpression of *cebpβ* and its target genes. Expression analysis revealed infection-responsive expression of *cebpβ* colocalized with *irg1*$^+$ macrophage-lineage cells within the midbrain and hindbrain (Figure 2E) and circulation (Figure 2F). Examining *cebpβ* expression within infected Irf8-depleted larvae further supported infection-responsive expression of *cebpβ* as being macrophage-lineage specific (Figures 2G and 2H). Assessing *irg1* expression within infected C/ebpβ-depleted larvae revealed that, despite maintaining typical numbers of macrophage-lineage cells (Figure S2B), *irg1* expression was almost completely abolished (Figures 2I–2K). Further support for the genetic positioning of Irg1 downstream of C/ebpβ was provided by showing infection-responsive *cebpβ* expression to be independent of Irg1 (Figures S2C–S2E).

These results reveal that the primary-response transcription factor C/ebpβ helps drive infection-responsive *irg1* expression within macrophage-lineage cells (Figure 2L). Of note, ectopic delivery of *cebpβ* mRNAs into zebrafish embryos (that we have previously shown can drive ectopic expression of target genes [Hall et al., 2012]) did not result in *irg1* missexpression (data not shown), suggesting that, although required, C/ebpβ is not sufficient to drive *irg1* expression. C/ebpβ-driven expression of *irg1* is most likely dependent on cooperation with other infection-responsive transcriptional regulators.

Glucocorticoid Receptor Signaling Promotes *irg1* Expression through Its Direct Regulation of *cebpβ* Expression

Analysis of the promoter region of zebrafish *cebpβ* revealed several consensus glucocorticoid (GC) response elements (GREs) (Figure S3A). Importantly, GC has been demonstrated to induce *C/EBPβ* expression within minutes of stimulation, independent of new protein synthesis (Hazra et al., 2007). We investigated whether the rapid onset of *irg1* expression within stimulated macrophage-lineage cells was dependent upon GC-driven expression of *cebpβ*.

To assess the requirement for endogenous GR-mediated signaling during infection-responsive *irg1* expression, infected larvae were treated with the GR antagonist RU-486 and *irg1* expression examined. RU-486-treated infected larvae demonstrated a dose-dependent reduction in the number of *irg1*$^+$ cells, when compared with infected DMSO-treated controls (Figures 3A–3C). Depleting larvae of the zebrafish ortholog of NR3C1 (encoding the GR) resulted in a similar reduction of *irg1* expression in response to infection (Figures 3D–3F and Figure S3B). Nr3c1 depletion also resulted in reduced infection-responsive *cebpβ* expression within macrophage-lineage cells (Figures 3G and 3H). Of note, Nr3c1-depleted larvae maintained typical numbers of macrophage-lineage cells (Figure S2B). Following infection, Nr3c1 protein was detected in the nucleus of macrophage-lineage cells (Figure 3I). The stress response of mammals is in part mediated through the production of endogenous GC by the adrenal gland. In zebrafish, the interrenal tissue functions as

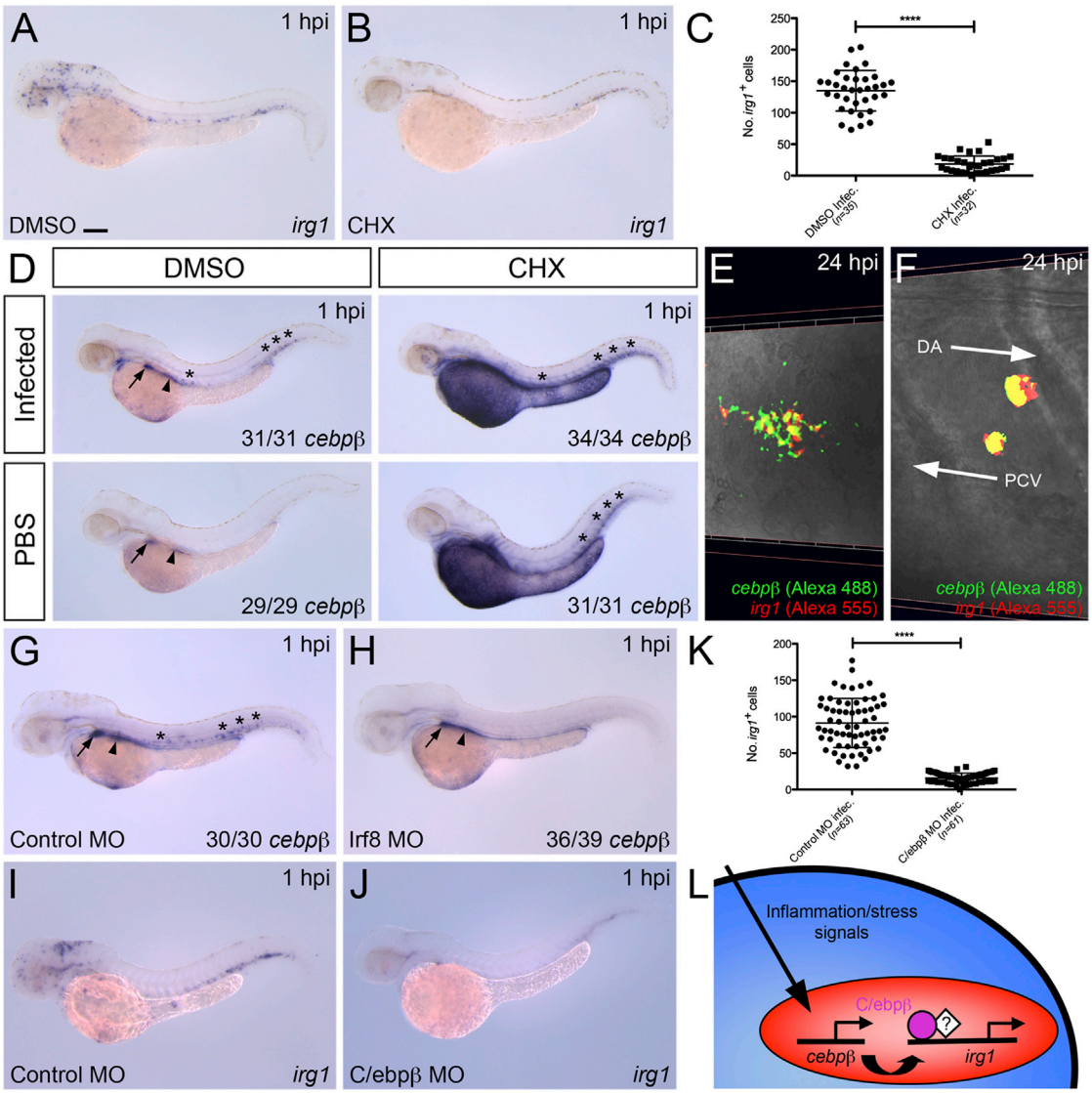

Figure 2. Infection-Responsive Expression of *irg1* within Macrophage-Lineage Cells Is Dependent on the Primary Response Transcription Factor C/ebpβ

(A and B) Expression of *irg1* within infected DMSO (control)- and CHX-treated larvae, respectively, at 1 hpi.

(C) Quantification of *irg1*$^+$ cells within individual infected larvae as shown in (A) and (B) (mean ± SD).

(D) Expression of *cebpβ* within DMSO (control)- and CHX-treated larvae, following infection or PBS injection, at 1 hpi.

(E and F) Dual expression analysis of *irg1* and *cebpβ* within the midbrain/hindbrain and trunk, respectively, of infected larvae at 24 hpi.

(G and H) Expression of *cebpβ* within infected control MO-injected and Irf8-depleted larvae, respectively, at 1 hpi.

(I and J) Expression of *irg1* within infected control MO-injected and C/ebpβ-depleted larvae, respectively, at 1 hpi.

(K) Quantification of *irg1*$^+$ cells within individual infected larvae as shown in (I) and (J) (mean ± SD).

(L) Schematic illustrating proposed regulation of infection-responsive *irg1* expression within macrophage-lineage cells. Asterisks, arrows, and arrowheads mark blood-specific, liver-specific, and gut-specific *cebpβ* expression, respectively. All views anterior to left. Numbers represent frequency of larvae with displayed phenotype. Scale bar, 100 μm in (A). Abbreviations: DA, dorsal aorta; PCV, posterior cardinal vein; ****$p < 0.0001$. See also Figure S2.

the adrenal gland equivalent and is the major site of steroidogenesis (Liu, 2007). Interrenal cells within embryos can be specifically ablated through knockdown of Nr5a1a (Liu, 2007). In addition to depleting larvae of functional markers of steroidogenesis (such as *cyp11a1*), Nr5a1a-depleted larvae also demonstrated marked reduction of *irg1*$^+$ cells following infection, despite maintaining typical numbers of macrophage-lineage cells (Figures S2B and S3C–S3G). To investigate whether exogenously supplied GR agonists were sufficient to induce *cebpβ* and *irg1*, dexamethasone, hydrocortisone, or prednisolone was injected into the hindbrain ventricle of 2 dpf larvae and *cebpβ* or *irg1* expression examined. In contrast to *irg1*, *cebpβ* expression within macrophage-lineage cells was strongly induced in response to GR agonist injection (Figures 3J and 3K).

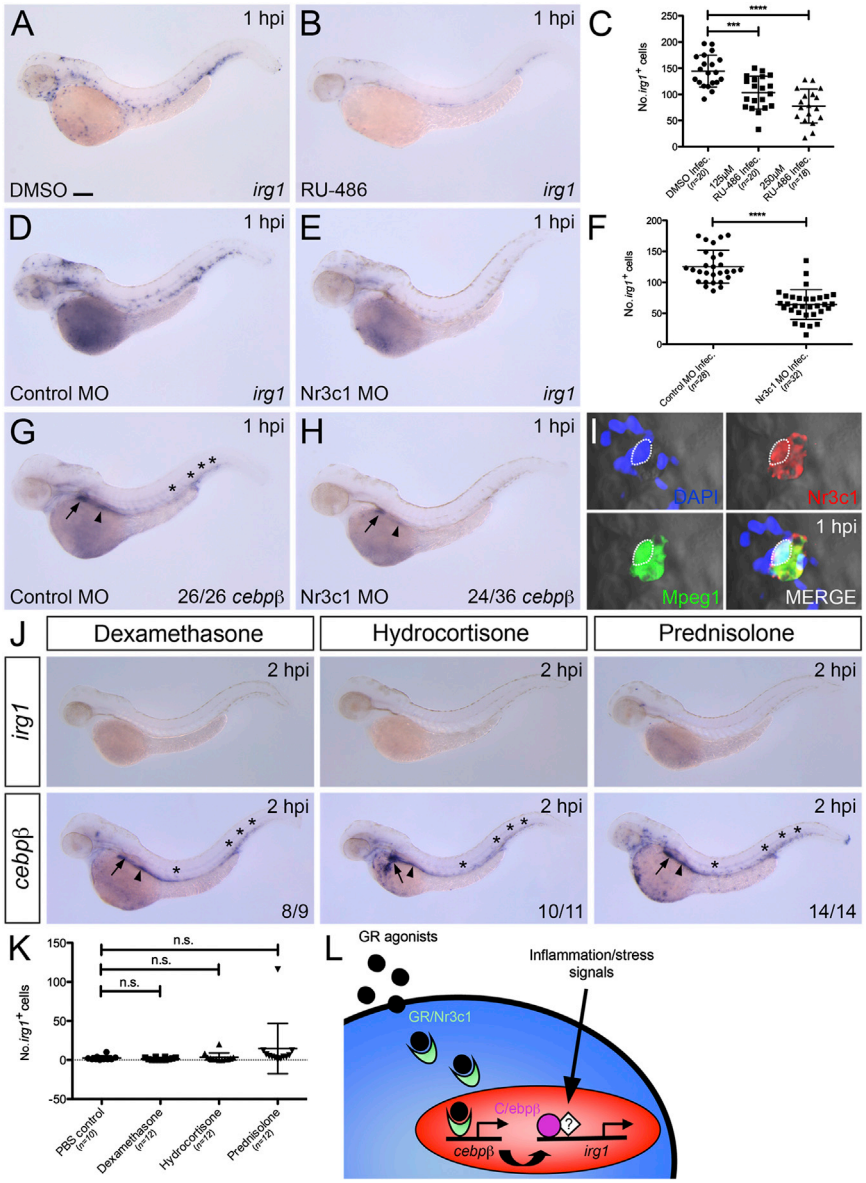

Figure 3. Glucocorticoid Receptor-Mediated Signaling Helps Regulate Infection-Responsive *irg1* Expression within Macrophage-Lineage Cells through Induction of *cebpβ* Expression

(A and B) Expression of *irg1* within infected DMSO (control)- and RU-486-treated (250 μM) larvae, respectively, at 1 hpi.

(C) Quantification of *irg1*$^+$ cells within individual infected larvae treated with DMSO (control), 125 μM RU-486, or 250 μM RU-486 (mean ± SD).

(D and E) Expression of *irg1* within infected control MO-injected and Nr3c1-depleted larvae, respectively, at 1 hpi.

(F) Quantification of *irg1*$^+$ cells within individual larvae as shown in (D) and (E) (mean ± SD).

(G and H) Expression of *cebpβ* within infected control MO-injected and Nr3c1-depleted larvae, respectively, at 1 hpi.

(I) Immunofluorescence detection of Nr3c1 (Alexa 546) and Mpeg1/EGFP (Alexa 488) within DAPI-stained infected macrophage-lineage marking *Tg(mpeg1:EGFP)* larvae at 1 hpi. Dashed line marks Nr3c1$^+$ nucleus.

(J) Expression of *irg1* and *cebpβ* within dexamethasone-, hydrocortisone-, and prednisolone-injected larvae at 2 hpi.

(K) Quantification of *irg1*$^+$ cells within individual larvae as shown in (J) (mean ± SD).

(L) Schematic illustrating proposed regulation of infection-responsive *irg1* expression within macrophage-lineage cells. Asterisks, arrows, and arrowheads mark blood-specific, liver-specific, and gut-specific *cebpβ* expression, respectively. All views anterior to left. Numbers represent frequency of larvae with displayed phenotype. Scale bar, 100 μm in (A). Abbreviations: ***p < 0.001; ****p < 0.0001; n.s., not significant. See also Figure S3.

These results reveal that the GC/GR signaling pathway helps control infection-responsive *cebpβ* expression within macrophage-lineage cells and that additional infection/stress-responsive pathways contribute to *irg1* expression (Figure 3L).

The JAK/STAT Pathway Cooperates with GR Signaling to Regulate *irg1* Expression in Response to Infection

Given the synergistic regulation of acute phase proteins by members of the C/EBP and cytokine-responsive STAT transcription factor families (Arambasić et al., 2010; Kordula and Travis, 1996), we investigated whether the JAK/STAT pathway contributes to *irg1* expression.

Analysis of the promoter region of zebrafish *irg1* revealed a number of STAT consensus binding motifs (Figure S4A). In addition, qPCR analysis of cytokine expression levels following infection revealed a number to be rapidly expressed with similar temporal kinetics to that of *irg1* (Figure S4B). To examine a requirement for JAK/STAT signaling during infection-responsive *irg1* expression, we utilized the cell-permeable JAK inhibitor AG490 and the STAT3-specific inhibitor (STAT3 inhibitor peptide/PpYLKTK-mts) (Funakoshi-Tago et al., 2011; Turkson et al., 2001). Both AG490- and STAT3 inhibitor-treated larvae demonstrated a dose-dependent decrease in the number of *irg1*$^+$ cells following infection, compared to DMSO-treated controls (Figures 4A–4D). A similar reduction in the number of *irg1*$^+$ cells was observed within infected Stat3-depleted larvae, despite maintaining typical numbers of macrophage-lineage cells, when compared to controls (Figures 4E–4G and Figure S2B). This was in contrast to infection-responsive *cebpβ* expression that remained unaffected following Stat3 depletion (Figures 4H and 4I). In addition, phosphorylated Stat3, as detected by immunofluorescence, was only observed within macrophage-lineage cells following infection (Figures 4J–4L). Consistent with the cooperative activities of GR- and JAK/STAT-mediated signaling on *irg1* expression, depletion of both Stat3 and Nr3c1 had a cumulative effect on reducing infection-responsive *irg1* expression (Figures 4M–4O).

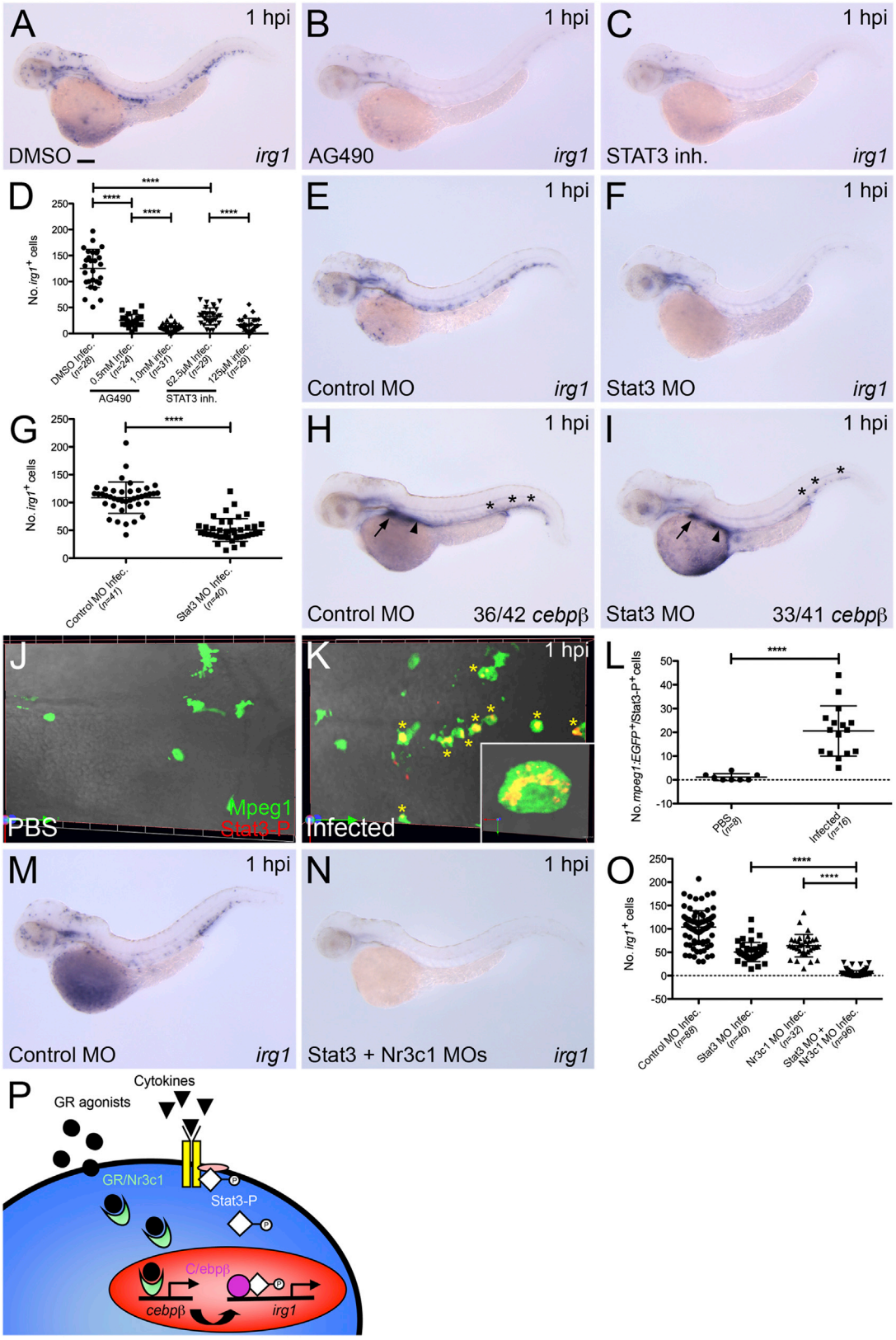

(legend on next page)

These data show that infection-responsive *irg1* expression within macrophage-lineage cells requires both the GR and JAK/STAT signaling pathways (Figure 4P).

Irg1-Depleted Macrophage-Lineage Cells Demonstrate Reduced Bacterial Activity

In support of a bactericidal activity for macrophage-lineage cells in our infection system, Irf8-depleted larvae were highly susceptible to even a low-dose infection challenge, when compared with controls (Figure S1E). To address whether Irg1 contributes to this bactericidal macrophage activity, we monitored bacterial persistence within Irg1-depleted larvae infected with GFP-expressing *Salmonella* (hereafter referred to as Sal-GFP). Irg1-depleted larvae demonstrated a significant increase in bacterial persistence, as assessed by live fluorescence microscopy (Figures 5A and 5B) and CFU counts/infected larva (Figure 5C), when compared with control larvae. This enhanced persistence was associated with a decrease in survival postinfection (Figure 5D). We next live imaged the intracellular bacterial burden within individual macrophage-lineage cells marked within *Tg(mpeg1:mCherry)* larvae (Ellett et al., 2011) following Sal-GFP injection (measured as the volume of GFP fluorescence signal within Mpeg1:mCherry$^+$ cells). This revealed that Irg1-depleted macrophage-lineage cells contained significantly elevated bacterial loads, when compared to controls, suggesting a defect in bactericidal activity (Figures 5E–5G). Of note, Irg1-depleted infected larvae maintained similar numbers of macrophage-lineage cells within the midbrain/hindbrain injection region, as measured at 3 hpi, when compared to control MO-injected infected larvae (Figures S5A–S5C).

A recent study has demonstrated the ability to directly observe and measure the bactericidal activity of fluorescent neutrophils infected with *Mycobacterium marinum* (Mm) by live imaging infected zebrafish larvae (Yang et al., 2012). By measuring the change in intracellular bacterial burden of red fluorescent Mm (quantified as a volume of intracellular fluorescence signal) within individual tracked green fluorescent neutrophils over time, a "killing rate" ($\Delta\mu m^3$/min) was calculated (Yang et al., 2012). We performed a similar analysis to track infected macrophage-lineage cells following Sal-GFP injection into Irg1-depleted and control MO-injected *Tg(mpeg1:mCherry)* larvae. This revealed that Irg1-depleted macrophage-lineage cells were defective in killing phagocytozed Sal-GFP, when compared to controls (Figures 5H and 5I).

These results confirm that enhanced susceptibility of Irg1-depleted larvae to infection is, at least in part, the result of reduced Irg1-dependent bactericidal activity of macrophage-lineage cells.

Irg1-Depleted Macrophage-Lineage Cells Demonstrate Defective Mitochondrial ROS Production in Response to Infection

Mitochondria have been shown to actively recruit to phagosomes containing phagocytozed bacteria where elevated mROS production enhances ROS-mediated bacterial killing (West et al., 2011a). Live imaging Sal-GFP-infected macrophage-lineage cells within *Tg(mpeg1:mCherry)* larvae coinjected with the mitochondria-marking MitoTracker probe revealed similar clustering of mitochondria around phagocytozed bacteria (Figures S6A–S6C). In light of the mitochondrial localization of IRG1 (Degrandi et al., 2009), we investigated a potential role for Irg1 during mROS production.

To directly observe and quantify mROS, we took advantage of the MitoSOX red mitochondrial superoxide indicator that specifically detects ROS produced within mitochondria. Coinjection of *Salmonella* with MitoTracker and MitoSOX probes into macrophage-lineage marking *Tg(mpeg1:EGFP)* larvae (Ellett et al., 2011) confirmed that MitoSOX fluorescence was specific to the mitochondria (Figures 6A and 6B). Quantifying mROS production as the total fluorescence intensity within individual macrophage-lineage cells within MitoSOX/*Salmonella*-coinjected *Tg(mpeg1:EGFP)* larvae revealed a significant increase in mROS when compared to MitoSOX/PBS-injected controls (Figures 6C and 6E). Similar analysis within Irg1-depleted larvae confirmed that infection-responsive mROS production was Irg1 dependent (Figures 6D and 6E) and could be partially rescued following *irg1* overexpression (Figure 6E and Figures S6D and S6E). These results confirm that macrophage-lineage mROS is generated in response to infection through an Irg1-dependent mechanism.

Figure 4. JAK/STAT Pathway Cooperates with Glucocorticoid Receptor-Mediated Signaling to Regulate Infection-Responsive *irg1* Expression within Macrophage-Lineage Cells

(A–C) Expression of *irg1* within infected DMSO (control)-, AG490 (0.5 mM)-, and STAT3 inhibitor peptide (62.5 μM)-treated larvae, respectively, at 1 hpi.

(D) Quantification of *irg1*$^+$ cells within individual infected larvae treated with DMSO, AG490 (0.5 and 1.0 mM), or STAT3 inhibitor peptide (62.5 and 125 μM), at 1 hpi (mean ± SD).

(E and F) Expression of *irg1* within infected control MO-injected and Stat3-depleted larvae, respectively, at 1 hpi.

(G) Quantification of *irg1*$^+$ cells within individual infected larvae as shown in (E) and (F) (mean ± SD).

(H and I) Expression of *cebpβ* within infected control MO-injected and Stat3-depleted larvae, respectively, at 1 hpi.

(J and K) Immunofluorescence detection of phosphorylated Stat3 (Stat3-P, Alexa 568) and Mpeg1/EGFP (Alexa 488) within the midbrain/hindbrain region of PBS-injected and infected *Tg(mpeg1:EGFP)* larvae, respectively, at 1 hpi. Yellow asterisks mark macrophage-lineage cells containing phosphorylated Stat3.

(L) Quantification of Stat3-P$^+$ macrophage-lineage cells within the midbrain/hindbrain region of individual larvae as shown in (J) and (K) (mean ± SD). Region assessed, 100 μm from dorsal-most surface of midbrain/hindbrain (512 × 512, 50 z sections at 2 μm).

(M and N) Expression of *irg1* within infected control MO-injected and Stat3 + Nr3c1-depleted larvae, respectively, at 1 hpi.

(O) Quantification of *irg1*$^+$ cells within individual infected control MO-injected, Stat3-depleted, Nr3c1-depleted, and Stat3 + Nr3c1-depleted larvae, at 1 hpi (mean ± SD).

(P) Schematic illustrating proposed regulation of infection-responsive *irg1* expression within macrophage-lineage cells. Asterisks, arrows, and arrowheads mark blood-specific, liver-specific, and gut-specific *cebpβ* expression, respectively. All views anterior to left. Numbers represent frequency of larvae with displayed phenotype. Scale bar, 100 μm in (A). ****$p < 0.0001$. See also Figure S4.

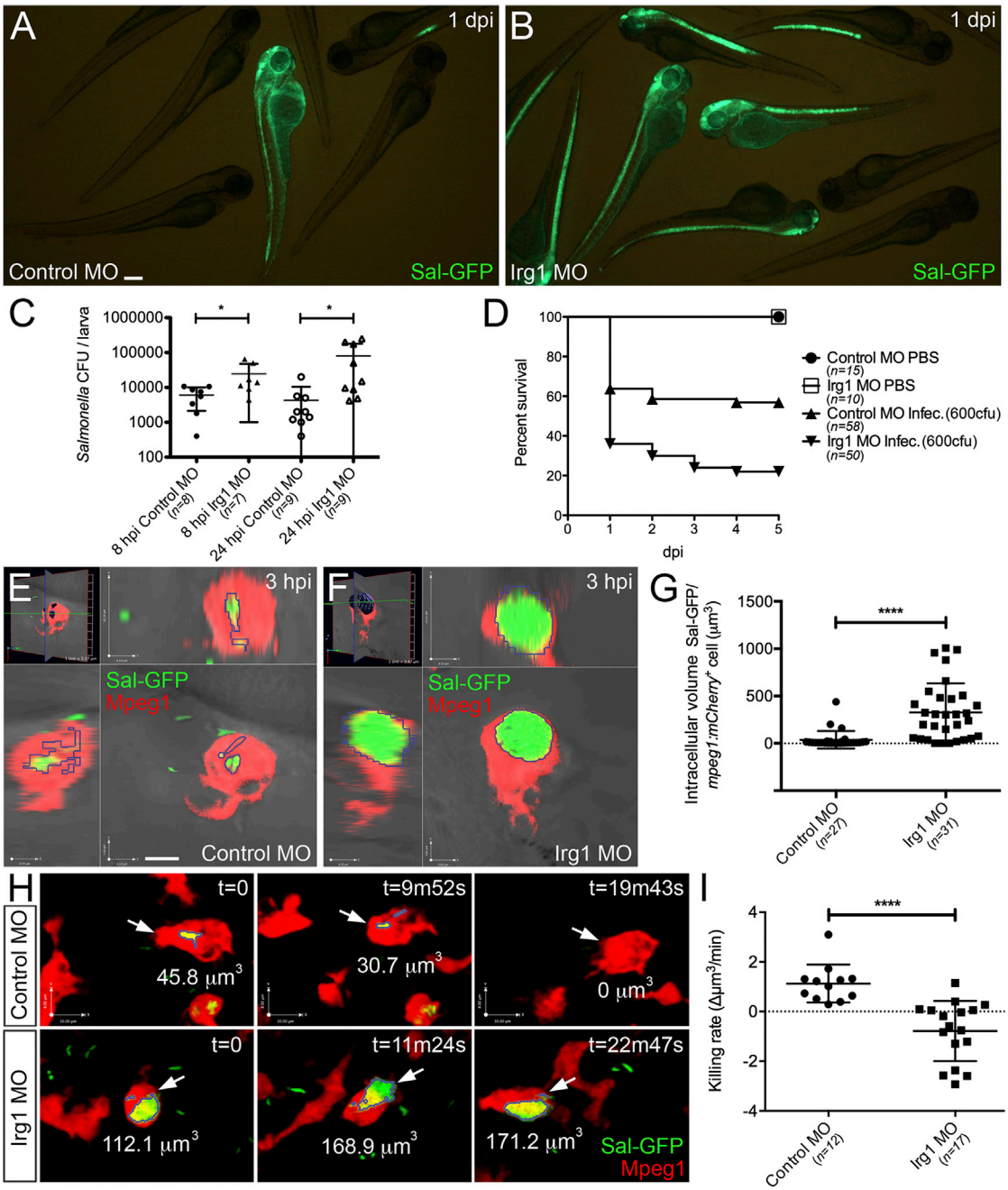

Figure 5. Irg1-Depleted Macrophage-Lineage Cells Demonstrate Diminished Bactericidal Activity

(A and B) Live imaging of control MO-injected and Irg1-depleted larvae, respectively, following infection with Sal-GFP, imaged at 1 dpi.

(C) CFU counts of remaining Sal-GFP within individual infected control MO-injected and Irg1-depleted larvae quantified at 8 and 24 hpi (mean ± SD).

(D) Survival graph demonstrating percentage survival of control MO-injected PBS-injected, Irg1-depleted PBS-injected, control MO-injected infected, and Irg1-depleted infected larvae from 1 to 5 dpi.

(E and F) Live confocal imaging of Sal-GFP within macrophage-lineage cells (within the midbrain/hindbrain region) of control MO-injected and Irg1-depleted *Tg(mpeg1:mCherry)* larvae, at 3 hpi, respectively.

(G) Quantification of intracellular Sal-GFP burden within individual macrophage-lineage cells as shown in (E) and (F) (measured as total intracellular volume of Sal-GFP per *mpeg1*$^+$ cell, mean ± SD).

(H) Representative frames from live time-lapse confocal imaging of Sal-GFP infected macrophage-lineage cells within the midbrain/hindbrain region of control MO-injected and Irg1-depleted larvae (imaging starts at 3 hpi). White arrows mark tracked infected macrophage-lineage cell. Intracellular bacterial volume within tracked cells is displayed as μm^3 within each time point.

(I) Quantification of killing rate (change in Sal-GFP bacterial volume/time, $\Delta\mu m^3$/min) of tracked infected macrophage-lineage cells, as shown in (H) (mean ± SD). Scale bars, 200 μm in (A); 5 μm in (E). *$p < 0.05$; ****$p < 0.0001$. See also Figure S5.

Irg1-Dependent Mitochondrial ROS Production in Response to Infection Is Dependent on Fatty Acid β-Oxidation

Immune cells have the capacity to fuel OXPHOS through glycolysis or fatty acid β-oxidation to support cell function (Pearce and Pearce, 2013). To determine whether infection-responsive mROS production within macrophage-lineage cells was dependent upon either glucose or fatty acid catabolism, we examined mROS production in the presence of chemical inhibitors of glycolysis and β-oxidation.

Treatment with the glycolysis inhibitor 2-deoxy-d-glucose (2-DG) (Suganuma et al., 2010) resulted in no significant decrease in mROS production (Figures 6F, 6G, and 6I). This was in contrast to treatment with etomoxir, an inhibitor of carnitine palmitoyltransferase-1 (Cpt1) (Vickers, 2009), a rate-limiting enzyme essential for β-oxidation, which inhibited mROS production in a dose-dependent manner (Figures 6F, 6H, and 6I). To assess the contribution of β-oxidation to the inflammatory response, etomoxir was coinjected with Sal-GFP, followed by analysis of bacterial persistence and larval survival. Etomoxir treatment effected a dose-dependent reduction in the ability of infected larvae to clear microinjected bacteria, when compared with DMSO-treated controls (Figures S6F and S6G). This bacterial persistence was associated with a decrease in survival postinfection (Figure S6H), similar to that observed within Irg1-depleted larvae (Figures 5A–5D).

These results suggest that during infection the mitochondria of macrophage-lineage cells employ β-oxidation to fuel mitochondrial respiration and the resulting production of Irg1-dependent mROS.

Mitochondria of Stimulated Macrophage-Lineage Cells Demonstrate Enhanced Fatty Acid Uptake

To investigate whether macrophage-lineage cells enhance their uptake of fatty acids to fuel mROS production in response to infection, we investigated the subcellular distribution of fluorescent fatty acids within LPS-stimulated macrophage-lineage cells. The fluorescent fatty acid analog BODIPY FL C_{16} has previously been used to image fatty acid uptake, accumulation, and transport in both human cells and live zebrafish larvae (Carten et al., 2011; Thumser and Storch, 2007).

To live image subcellular accumulation of BODIPY FL C_{16}, we took advantage of its ability to shift fluorescence emission from green to red when detected at concentrations sufficient to induce excimer formation (Carten et al., 2011). Confocal imaging using a ratio channel (red/green) then enabled areas of highly concentrated BODIPY FL C_{16} to be live imaged. Following coinjection of BODIPY FL C_{16}, LPS, and MitoTracker into the hindbrain ventricle, we detected subcellular regions of highly concentrated BODIPY FL C_{16} within macrophage-lineage cells (as detected by morphology) (Figure S7A). Line intensity profiling confirmed that areas of maximum BODIPY FL C_{16} concentration were localized to the mitochondria (Figures S7A and S7B). Measuring peak fluorescence intensity ratios within individual macrophage-lineage cells following coinjection of BODIPY FL C_{16} with LPS or PBS showed BODIPY FL C_{16} only concentrated within the mitochondria of LPS-stimulated macrophage-lineage cells (Figures S7C, S7D, and S7G). Transportation of fatty acids across the outer mitochondrial membrane into the mitochondrial matrix is regulated by the rate-limiting enzyme Cpt1. Repeating the above experiment in the presence of coinjected etomoxir demonstrated that LPS-stimulated trafficking of BODIPY FL C_{16} into the mitochondria was dependent on Cpt1-mediated transport (Figures S7E–S7G).

Fatty Acid Supplementation Can Enhance Macrophage-Lineage mROS Production in Response to Infection, but Not Following Irg1 Depletion

We next evaluated whether exogenously supplied fatty acids could enhance the production of mROS within macrophage-lineage cells. Coinjecting an equimolar mixture of several saturated fatty acids with *Salmonella* resulted in elevated production of mROS within macrophage-lineage cells, when compared with *Salmonella* injection alone (Figures 7A–7C). A similar increase was not detected within Irg1-depleted larvae (Figure 7C). Microinjection of exogenous fatty acids also enhanced the clearance of coinjected Sal-GFP, when compared with Sal-GFP injection alone (Figures S7H–S7J). Of note, overexpression of *irg1* was not sufficient to elevate mROS within macrophage-lineage cells, even following fatty acid supplementation (Figure S7K).

These data show that exogenously supplied fatty acids can enhance the production of infection-responsive mROS within macrophage-lineage cells and the clearance of injected bacteria. Furthermore, the utilization of exogenous fatty acids to enhance mROS requires Irg1.

LPS-Induced Mitochondrial ROS Production and Bactericidal Activity within Murine Macrophages Are Dependent on Fatty Acid β-Oxidation

We next investigated whether β-oxidation-dependent mROS production was conserved within stimulated mammalian macrophages and whether it contributed to bactericidal activity. Consistent with our studies in zebrafish larvae, etomoxir-treated J774.2 cells were defective in mROS production (in response to LPS) and bactericidal activity toward intracellular Sal-GFP (Figures 7D–7F). Importantly, these effects of etomoxir were not the result of a general/nonspecific impairment of cell health or immune response, as evidenced by unaffected elevated expression of *Irg1* and the proinflammatory cytokines *TNF-α* and *IL-12p40* (Figure S7L). Of note, stimulation of J774.2 cells with LPS resulted in elevated *Irg1* expression (Figure S7M) and the detection of IRG1 protein at the mitochondria (Figure S7N).

DISCUSSION

Taking advantage of live imaging techniques within an intact animal model system, we reveal Irg1 as a critical component of the immunometabolism axis connecting infection, mitochondrial metabolism, and macrophage function. We show that expression of Irg1, an infection-responsive enzyme known to localize to the mitochondria, is dependent on the cooperative activities of both the GR and JAK/STAT signaling pathways and the transcription factors C/ebpβ and Stat3. We further reveal Irg1 to be essential for infection-responsive mROS production, a process dependent on enhanced mitochondrial uptake and β-oxidation of fatty acids. Defective mROS and its associated bactericidal activity contribute to impaired bacterial clearance by Irg1-deficient macrophage-lineage cells (Figure 7G). We

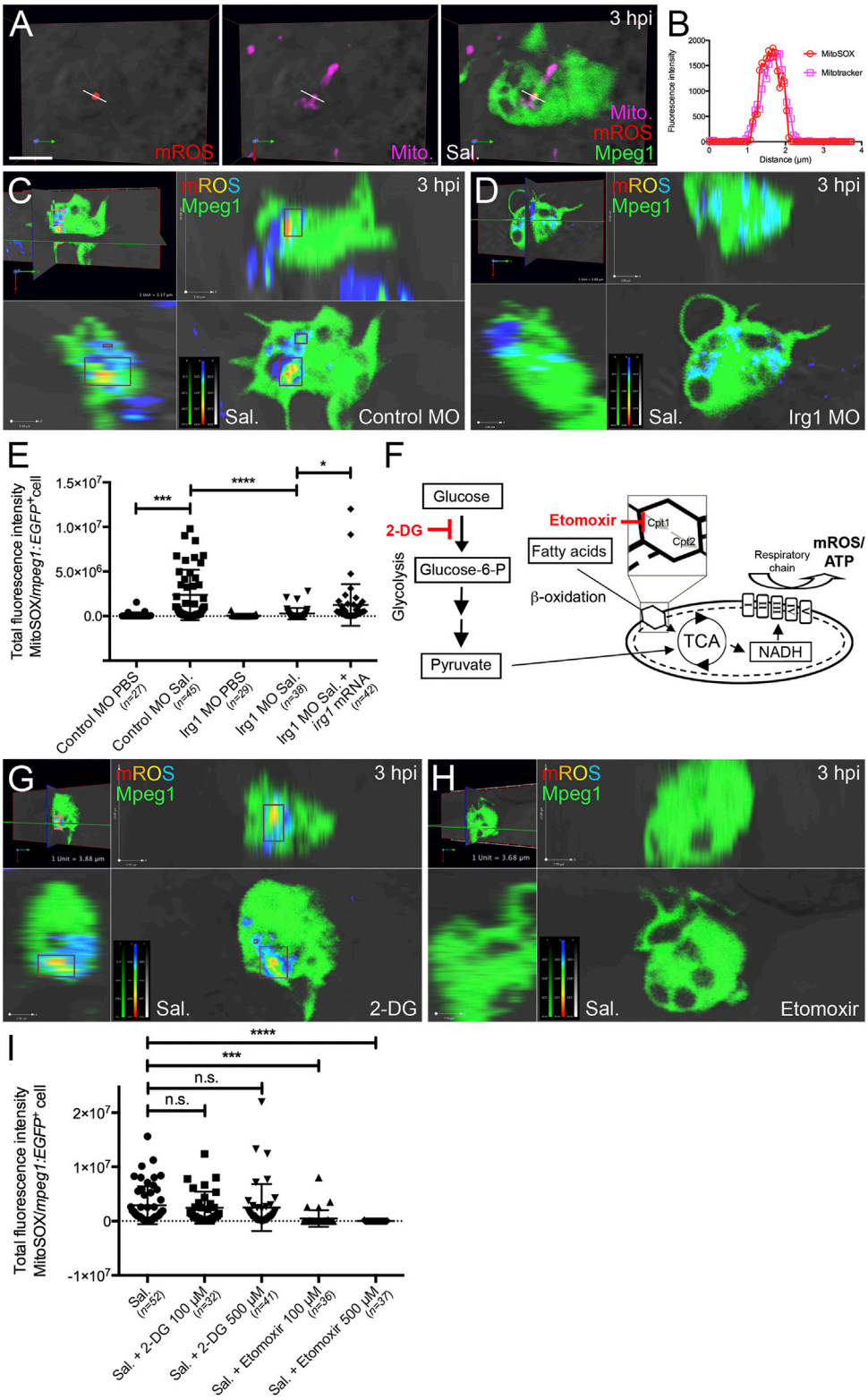

Figure 6. mROS Production within Macrophage-Lineage Cells Is Dependent on Irg1 and Fatty Acid β-Oxidation

(A) Live confocal imaging of mROS production by macrophage-lineage cells within the midbrain/hindbrain region of *Tg(mpeg1:EGFP)* larvae at 3 hpi (following injection of *Salmonella* (Sal.), MitoSOX, and MitoTracker mitochondria-marking probes).

(B) Line intensity profiles for MitoSOX and MitoTracker (for line shown in A) demonstrating overlapping signals and specificity of MitoSOX to the mitochondria of macrophage-lineage cells.

(legend continued on next page)

also demonstrate the conserved dependence on fatty acid β-oxidation for mROS production and bactericidal activity within stimulated murine macrophages.

It has long been recognized that professional phagocytes produce ROS as part of their effector response to help eliminate intracellular bacteria. These intracellular bactericidal ROS were primarily believed to result from the activity of phagosomal superoxide-generating NADPH oxidases (NOX) (Rada and Leto, 2008). It is now apparent that mROS production, a consequence of electron transport through OXPHOS complexes and a major source of cellular ROS, increases following infection and directly contributes to clearing bacteria from infected macrophages (Roca and Ramakrishnan, 2013; West et al., 2011a, 2011b). Mitochondria have been shown to associate with phagosomes containing intracellular bacteria (Chong et al., 2009; Sinai et al., 1997). In an important study, West and colleagues demonstrate that the consequence of this mitochondrial trafficking is to deliver bactericidal ROS into the phagosome to enhance the clearance of intracellular bacteria (West et al., 2011a). The authors propose this mROS bactericidal contribution acts in concert with NOX-derived ROS to effect full ROS generation within the phagosome (West et al., 2011a). Our live imaging data support this emerging role for mROS in contributing to the clearing of intracellular bacteria within infected macrophages. We show that both zebrafish and murine macrophages utilize fatty acids to "fuel" mROS production that contributes to the clearance of intracellular bacteria. We demonstrate that this mROS production is dependent on infection-responsive expression of the mitochondria-localizing enzyme Irg1, which is also required for the utilization of fatty acids as a fuel to help augment mROS production. Our data show that Irg1, although required, is not sufficient to drive mROS production in the absence of infection, even in the presence of enhanced fatty acid availability. This suggests that Irg1 acts in concert with other infection-responsive metabolic machinery to facilitate the utilization of fatty acids during β-oxidation-driven mROS production.

The infection-responsive capacity of mitochondria to potentiate OXPHOS-derived mROS production suggests they possess enhanced OXPHOS capacity, either through elevated mitochondrial biogenesis and/or upregulated production/activity of OXPHOS components. Macrophage activation by interferon-γ has been demonstrated to enhance expression of several OXPHOS components through activation of estrogen-related receptor-α (ERRα) and peroxisome proliferator-activated receptor-γ co-activator 1β (PGC1β) (Sonoda et al., 2007). This signaling cascade contributes to increased mROS production and the efficient clearance of intracellular *Listeria monocytogenes*, linking inflammation-responsive elevation in macrophage mitochondrial respiratory capacity with mROS and bactericidal activity. The potential of cytokines to influence mitochondrial respiratory capacity has also been demonstrated within lymphocytes following infection. Interleukin-15-stimulated memory $CD8^+$ T cells possess considerable spare respiratory capacity (the capacity to generate extra ATP through OXPHOS to satisfy elevated energy demands) associated with increased mitochondrial biogenesis and enhanced fatty acid β-oxidation (van der Windt et al., 2012).

A master regulator of β-oxidation in the liver is the GC-responsive transcriptional coactivator PGC-1α. In support of GC and C/EBPβ as upstream regulators of Irg1, and the involvement of Irg1 during enhanced fatty acid catabolism, the activities of murine PGC-1α, Cpt1a (a PGC-1α target), and long-chain acyl-coenzyme A dehydrogenase (LDAC), all critical regulators of β-oxidation, have been shown to be C/EBPβ dependent within the regenerating liver (Wang et al., 2008). IRG1 has been described as the mammalian homolog of bacterial 2-methylcitrate dehydratase (Chen et al., 2003). This enzyme catalyzes a critical step during short-chain fatty acid metabolism in bacteria, to help fuel the TCA cycle (Brock et al., 2002). Recently it has been shown that Irg1 can catalyze production of itaconic acid, which possesses bactericidal activity (Michelucci et al., 2013). How the enzymatic activity of Irg1 (or downstream metabolites it may generate) is biochemically implicated during β-oxidation-driven mROS production is the focus of future research.

We propose that IRG1 functions as a critical regulator of macrophage function by helping regulate an increase in β-oxidation-"fueled" mROS production. In the context of bacterial infection, this mROS augments macrophage bactericidal capacity. However, as a signaling molecule, mROS can also influence effector function by altering the production and activity of different inflammatory cytokines (Naik and Dixit, 2011). Given the growing importance of mROS during the pathogenesis of conditions with an underlying inflammatory component, including diabetes, cancer, and neurodegenerative diseases, identifying new signaling systems that modulate its production holds therapeutic promise. IRG1 therefore represents a potential target for manipulation of the inflammation/metabolism interface.

EXPERIMENTAL PROCEDURES

Zebrafish Maintenance

The macrophage-lineage marking *Tg(mpeg1:mCherry)*^{gl23}, *Tg(mpeg1:Gal4)*^{gl24}; *Tg(UAS-E1b:Kaede)*^{s1999t} (herein referred to as *Tg[mpeg1:Gal4/UAS:kaede]*),

(C and D) Live confocal imaging of mROS production by macrophage-lineage cells within the midbrain/hindbrain region of control MO-injected and Irg1-depleted *Tg(mpeg1:EGFP)* larvae at 3 hpi, respectively, following *Salmonella* and MitoSOX injection. MitoSOX fluorescence intensity is displayed as a colormap, with warmer colors representing higher signal intensities.

(E) Quantification of mROS production by macrophage-lineage cells (measured as total fluorescence intensities of MitoSOX within individual *mpeg1*$^+$ cells), as marked in (C), within control MO-injected and Irg1-depleted *Tg(mpeg1:EGFP)* larvae at 3 hpi, following PBS or *Salmonella* (Sal.) injection (mean ± SD). For the rescue experiment, 300 pg *irg1* mRNA was coinjected with Irg1-targeting MOs. Five to ten larvae were sampled per treatment.

(F) Schematic illustrating glucose and fatty acids as alternate energy sources for mitochondrial respiration and associated mROS production. Points of activity for 2-DG (glycolysis inhibitor) and the β-oxidation inhibitor etomoxir (specific for Cpt1) are marked.

(G and H) Live confocal imaging of mROS production by macrophage-lineage cells within the midbrain/hindbrain region of *Tg(mpeg1:EGFP)* larvae at 3 hpi, following *Salmonella* (Sal.)/MitoSOX injection supplemented with 500 μM of 2-DG and etomoxir, respectively.

(I) Quantification of mROS production by macrophage-lineage cells (as measured in G and H) following indicated treatments (mean ± SD). Five to ten larvae were sampled per treatment. Scale bar, 5 μm in (A). Abbreviations: n.s., not significant; *$p < 0.05$; ***$p < 0.001$; ****$p < 0.0001$. See also Figure S6.

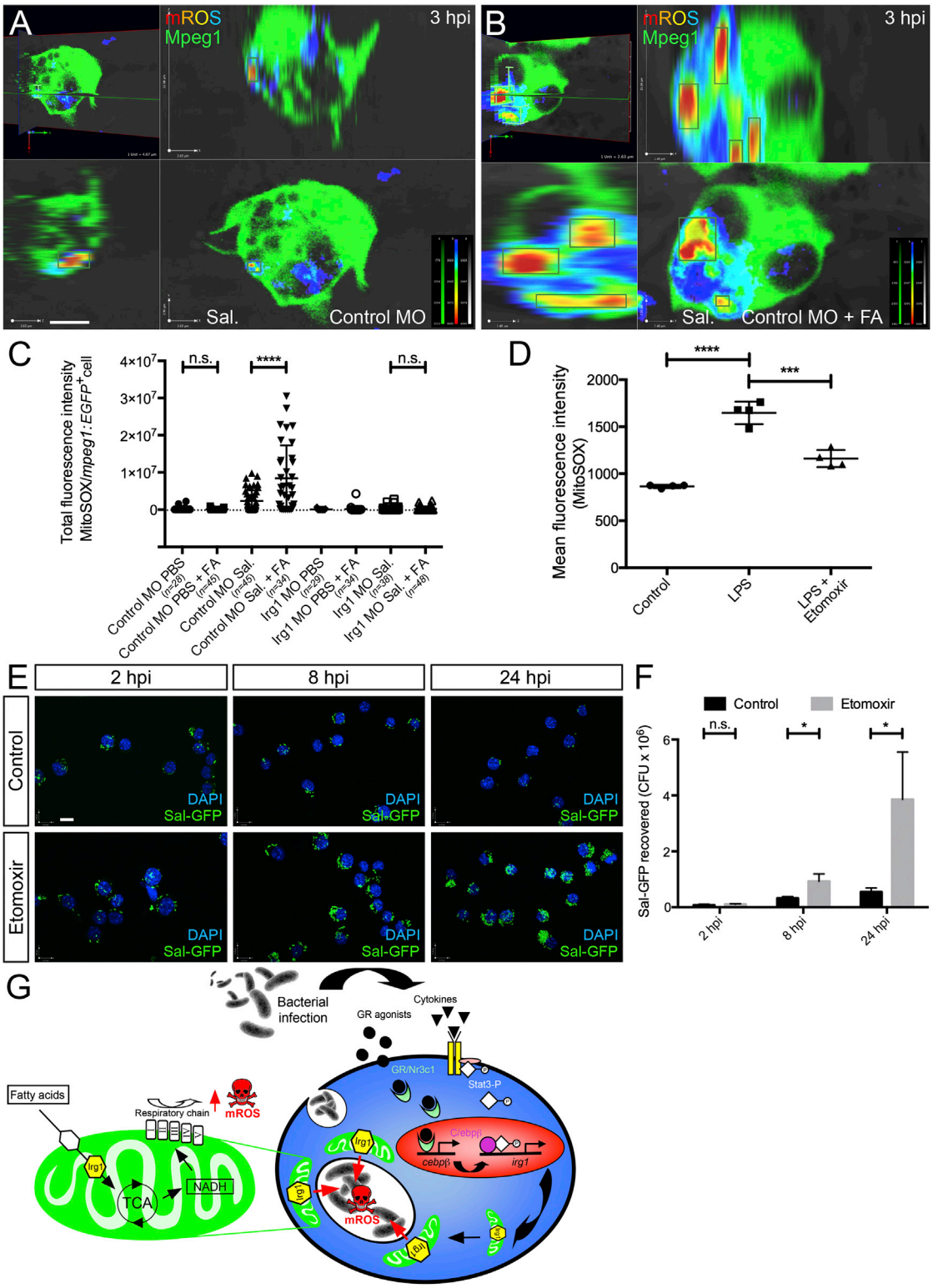

Figure 7. Irg1 Is Required for Enhanced mROS Production within Macrophage-Lineage Cells in Response to Fatty Acid Supplementation

Inhibition of β-oxidation reduces LPS-stimulated mROS production and bactericidal activity of J774.2 murine macrophage-like cells.

(A and B) Live confocal imaging of mROS production by macrophage-lineage cells within the midbrain/hindbrain region of control MO-injected *Tg(mpeg1:EGFP)* larvae, at 3 hpi, following *Salmonella* (Sal.)/MitoSOX injection alone or supplemented with an equimolar fatty acid mixture, respectively. MitoSOX fluorescence intensity is displayed as a colormap, with warmer colors representing higher signal intensities.

(legend continued on next page)

and *Tg(mpeg1:EGFP)*^{gl22} transgenic zebrafish (*Danio rerio*) were used in this study. Research was conducted with approval from The University of Auckland Animal Ethics Committee.

Infection of Zebrafish Larvae

Larvae were injected with wild-type or GFP-expressing *Salmonella* serovar Typhimurium into the hindbrain ventricle as previously described (Hall et al., 2012).

Whole-Mount In Situ Hybridization

Whole-mount in situ hybridizations were performed as previously described (Hall et al., 2012; Jowett and Lettice, 1994). To quantify *irg1*-expressing cells, larvae were mounted and viewed under Nomaski optics (10× objective) on a Leica DMRBE compound microscope.

RT-PCR

Total RNAs were extracted from embryos and larvae using TRIzol reagent (Invitrogen) and cDNAs generated using Superscript III reverse transcriptase (Invitrogen). Gene-specific amplicons were generated using the primer pairs listed in Table S1.

Morpholino Oligonucleotide Injection

Efficacious doses for all MOs (Gene Tools, Philomath, OR) were determined empirically. RT-PCR was used to determine MO specificity where splice-blocking MOs were used (see Table S2 for oligonucleotide sequences and doses).

Confocal Imaging

Live embryos and larvae were imaged as previously described (Hall et al., 2009b; Yang et al., 2012). Images were processed and analyzed using Volocity 6.1.1 (Perkin Elmer). See Table S3 for live imaging dyes/fluorescent probes used, their concentrations, and excitation/emission maxima.

Chemical Treatments

See Table S4 for drugs used, their targets, treatment doses, and mode of delivery. No abnormal development or toxicity was observed for all compounds used at the indicated working concentrations.

Quantitative PCR

QPCR was performed with Platinum SYBR Green qPCR SuperMix-UDG with ROX (Invitrogen) using an ABI PRISM 7900HT Fast sequence detection system (Applied Biosystems). Gene-specific oligonucleotides were designed using Primer Express software (see Table S1).

Statistical Analysis

Statistical analyses were performed using Prism 5.0 (GraphPad Software, Inc.). Statistical significance was assessed using unpaired, two-tailed t tests, and all data presented in scatter plots are mean ± SD. p values < 0.05 were considered statistically significant.

Immunofluorescence

Primary and secondary antibodies used are listed in Table S5.

Flow Cytometry

Flow cytometry was performed as previously described (Hall et al., 2009a).

Promoter Analysis

Putative transcription factor binding sites were identified using Genomatrix MatInspector software.

TLR and GR Agonist Injections

TLR (Human TLR Agonist Kit, InvivoGen) and GR agonists were injected into the hindbrain ventricle at 52 hpf. See Table S6 for microinjection doses. All agonists were diluted in filter-sterilized PBS.

Fatty Acid Injections

An equimolar ratio of fatty acids (Table S7) was microinjected into the hindbrain ventricle at 52 hpf.

Cell Culture and Gentamicin Protection Assay

J774.2 murine macrophage-like cells were maintained in RPMI 1640 (GIBCO, Life Technologies) supplemented with 10% fetal bovine serum and 5% antibiotic-antimycotic (GIBCO, Life Technologies). The gentamicin protection assay was performed essentially as described (West et al., 2011a).

Refer to the Supplemental Information for detailed experimental procedures.

SUPPLEMENTAL INFORMATION

Supplemental Information includes seven figures, seven tables, Supplemental Experimental Procedures, and Supplemental References and can be found with this article at http://dx.doi.org/10.1016/j.cmet.2013.06.018.

ACKNOWLEDGMENTS

We thank Sophie Wicker, Annie Chien, Pauline Misa, Alisha Malik, and Alhad Mahagaonkar for excellent technical assistance. The ARMI is supported by grants from the State Government of Victoria and the Australian Government. Funding for this work was provided by a grant awarded to P.S.C. from the MBIE, New Zealand.

Received: December 17, 2012
Revised: April 30, 2013
Accepted: June 26, 2013
Published: August 6, 2013

REFERENCES

Arambasić, J., Poznanović, G., Ivanović-Matić, S., Bogojević, D., Mihailović, M., Uskoković, A., and Grigorov, I. (2010). Association of the glucocorticoid receptor with STAT3, C/EBPbeta, and the hormone-responsive element within the rat haptoglobin gene promoter during the acute phase response. IUBMB Life *62*, 227–236.

Brock, M., Maerker, C., Schütz, A., Völker, U., and Buckel, W. (2002). Oxidation of propionate to pyruvate in Escherichia coli. Involvement of methylcitrate dehydratase and aconitase. Eur. J. Biochem. *269*, 6184–6194.

Carten, J.D., Bradford, M.K., and Farber, S.A. (2011). Visualizing digestive organ morphology and function using differential fatty acid metabolism in live zebrafish. Dev. Biol. *360*, 276–285.

Chen, B., Zhang, D., and Pollard, J.W. (2003). Progesterone regulation of the mammalian ortholog of methylcitrate dehydratase (immune response gene

(C) Quantification of mROS production by macrophage-lineage cells (measured as total fluorescence intensities of MitoSOX within individual *mpeg1*$^{+}$ cells), as marked in (A) and (B), within control MO-injected and Irg1-depleted *Tg(mpeg1:EGFP)* larvae at 3 hpi, following the indicated treatments (mean ± SD). Five to ten larvae were sampled for each treatment.
(D) Quantification of MitoSOX fluorescence, as detected by flow cytometry (measured as mean fluorescence intensity), within J774.2 murine macrophage-like cells treated with LPS alone (500 ng/ml) or supplemented with 50 μM etomoxir, compared to untreated, n = 4 biological replicates (mean ± SD).
(E) Gentamicin protection assay showing infected DAPI-stained J774.2 cells (either untreated (control) or treated with 50 μM etomoxir) at 2, 8, and 24 hr postinfection (hpi) with Sal-GFP.
(F) Quantification of recovered Sal-GFP following cell lysis and plating of samples, as shown in (E), n = 3 biological replicates (mean ± SD).
(G) Model for Irg1/β-oxidation-dependent bactericidal mROS production. Scale bars, 5 μm in (A) and (E). Abbreviations: n.s., not significant; *p < 0.05; ***p < 0.001; ****p < 0.0001. See also Figure S7.

1) in the uterine epithelium during implantation through the protein kinase C pathway. Mol. Endocrinol. *17*, 2340–2354.

Chong, A., Lima, C.A., Allan, D.S., Nasrallah, G.K., and Garduño, R.A. (2009). The purified and recombinant Legionella pneumophila chaperonin alters mitochondrial trafficking and microfilament organization. Infect. Immun. *77*, 4724–4739.

Degrandi, D., Hoffmann, R., Beuter-Gunia, C., and Pfeffer, K. (2009). The proinflammatory cytokine-induced IRG1 protein associates with mitochondria. J. Interferon Cytokine Res. *29*, 55–67.

Ellett, F., Pase, L., Hayman, J.W., Andrianopoulos, A., and Lieschke, G.J. (2011). mpeg1 promoter transgenes direct macrophage-lineage expression in zebrafish. Blood *117*, e49–e56.

Funakoshi-Tago, M., Tago, K., Sato, Y., Tominaga, S., and Kasahara, T. (2011). JAK2 is an important signal transducer in IL-33-induced NF-κB activation. Cell. Signal. *23*, 363–370.

Hall, C., Flores, M.V., Chien, A., Davidson, A., Crosier, K., and Crosier, P. (2009a). Transgenic zebrafish reporter lines reveal conserved Toll-like receptor signaling potential in embryonic myeloid leukocytes and adult immune cell lineages. J. Leukoc. Biol. *85*, 751–765.

Hall, C., Flores, M.V., Crosier, K., and Crosier, P. (2009b). Live cell imaging of zebrafish leukocytes. Methods Mol. Biol. *546*, 255–271.

Hall, C.J., Flores, M.V., Oehlers, S.H., Sanderson, L.E., Lam, E.Y., Crosier, K.E., and Crosier, P.S. (2012). Infection-responsive expansion of the hematopoietic stem and progenitor cell compartment in zebrafish is dependent upon inducible nitric oxide. Cell Stem Cell *10*, 198–209.

Hargreaves, D.C., Horng, T., and Medzhitov, R. (2009). Control of inducible gene expression by signal-dependent transcriptional elongation. Cell *138*, 129–145.

Hazra, A., DuBois, D.C., Almon, R.R., and Jusko, W.J. (2007). Assessing the dynamics of nuclear glucocorticoid-receptor complex: adding flexibility to gene expression modeling. J. Pharmacokinet. Pharmacodyn. *34*, 333–354.

Herbomel, P., Thisse, B., and Thisse, C. (2001). Zebrafish early macrophages colonize cephalic mesenchyme and developing brain, retina, and epidermis through a M-CSF receptor-dependent invasive process. Dev. Biol. *238*, 274–288.

Jowett, T., and Lettice, L. (1994). Whole-mount in situ hybridizations on zebrafish embryos using a mixture of digoxigenin- and fluorescein-labelled probes. Trends Genet. *10*, 73–74.

Kawai, T., Takeuchi, O., Fujita, T., Inoue, J., Mühlradt, P.F., Sato, S., Hoshino, K., and Akira, S. (2001). Lipopolysaccharide stimulates the MyD88-independent pathway and results in activation of IFN-regulatory factor 3 and the expression of a subset of lipopolysaccharide-inducible genes. J. Immunol. *167*, 5887–5894.

Kordula, T., and Travis, J. (1996). The role of Stat and C/EBP transcription factors in the synergistic activation of rat serine protease inhibitor-3 gene by interleukin-6 and dexamethasone. Biochem. J. *313*, 1019–1027.

Lee, C.G., Jenkins, N.A., Gilbert, D.J., Copeland, N.G., and O'Brien, W.E. (1995). Cloning and analysis of gene regulation of a novel LPS-inducible cDNA. Immunogenetics *41*, 263–270.

Li, L., Jin, H., Xu, J., Shi, Y., and Wen, Z. (2011). Irf8 regulates macrophage versus neutrophil fate during zebrafish primitive myelopoiesis. Blood *117*, 1359–1369.

Liu, Y.W. (2007). Interrenal organogenesis in the zebrafish model. Organogenesis *3*, 44–48.

Manfredi, A.A., and Rovere-Querini, P. (2010). The mitochondrion—a Trojan horse that kicks off inflammation? N. Engl. J. Med. *362*, 2132–2134.

Mathis, D., and Shoelson, S.E. (2011). Immunometabolism: an emerging frontier. Nat. Rev. Immunol. *11*, 81–83.

Matsuno, F., Chowdhury, S., Gotoh, T., Iwase, K., Matsuzaki, H., Takatsuki, K., Mori, M., and Takiguchi, M. (1996). Induction of the C/EBP beta gene by dexamethasone and glucagon in primary-cultured rat hepatocytes. J. Biochem. *119*, 524–532.

Michelucci, A., Cordes, T., Ghelfi, J., Pailot, A., Reiling, N., Goldmann, O., Binz, T., Wegner, A., Tallam, A., Rausell, A., et al. (2013). Immune-responsive gene 1 protein links metabolism to immunity by catalyzing itaconic acid production. Proc. Natl. Acad. Sci. USA *110*, 7820–7825.

Naik, E., and Dixit, V.M. (2011). Mitochondrial reactive oxygen species drive proinflammatory cytokine production. J. Exp. Med. *208*, 417–420.

Pearce, E.L., and Pearce, E.J. (2013). Metabolic pathways in immune cell activation and quiescence. Immunity *38*, 633–643.

Rada, B., and Leto, T.L. (2008). Oxidative innate immune defenses by Nox/Duox family NADPH oxidases. Contrib. Microbiol. *15*, 164–187.

Roca, F.J., and Ramakrishnan, L. (2013). TNF dually mediates resistance and susceptibility to mycobacteria via mitochondrial reactive oxygen species. Cell *153*, 521–534.

Semova, I., Carten, J.D., Stombaugh, J., Mackey, L.C., Knight, R., Farber, S.A., and Rawls, J.F. (2012). Microbiota regulate intestinal absorption and metabolism of fatty acids in the zebrafish. Cell Host Microbe *12*, 277–288.

Sinai, A.P., Webster, P., and Joiner, K.A. (1997). Association of host cell endoplasmic reticulum and mitochondria with the Toxoplasma gondii parasitophorous vacuole membrane: a high affinity interaction. J. Cell Sci. *110*, 2117–2128.

Sonoda, J., Laganière, J., Mehl, I.R., Barish, G.D., Chong, L.W., Li, X., Scheffler, I.E., Mock, D.C., Bataille, A.R., Robert, F., et al. (2007). Nuclear receptor ERR alpha and coactivator PGC-1 beta are effectors of IFN-gamma-induced host defense. Genes Dev. *21*, 1909–1920.

Suganuma, K., Miwa, H., Imai, N., Shikami, M., Gotou, M., Goto, M., Mizuno, S., Takahashi, M., Yamamoto, H., Hiramatsu, A., et al. (2010). Energy metabolism of leukemia cells: glycolysis versus oxidative phosphorylation. Leuk. Lymphoma *51*, 2112–2119.

Thumser, A.E., and Storch, J. (2007). Characterization of a BODIPY-labeled fluorescent fatty acid analogue. Binding to fatty acid-binding proteins, intracellular localization, and metabolism. Mol. Cell. Biochem. *299*, 67–73.

Turkson, J., Ryan, D., Kim, J.S., Zhang, Y., Chen, Z., Haura, E., Laudano, A., Sebti, S., Hamilton, A.D., and Jove, R. (2001). Phosphotyrosyl peptides block Stat3-mediated DNA binding activity, gene regulation, and cell transformation. J. Biol. Chem. *276*, 45443–45455.

van der Vaart, M., van Soest, J.J., Spaink, H.P., and Meijer, A.H. (2013). Functional analysis of a zebrafish myd88 mutant identifies key transcriptional components of the innate immune system. Dis. Model. Mech. *6*, 841–854.

van der Windt, G.J., Everts, B., Chang, C.H., Curtis, J.D., Freitas, T.C., Amiel, E., Pearce, E.J., and Pearce, E.L. (2012). Mitochondrial respiratory capacity is a critical regulator of CD8+ T cell memory development. Immunity *36*, 68–78.

Vickers, A.E. (2009). Characterization of hepatic mitochondrial injury induced by fatty acid oxidation inhibitors. Toxicol. Pathol. *37*, 78–88.

Wang, H., Peiris, T.H., Mowery, A., Le Lay, J., Gao, Y., and Greenbaum, L.E. (2008). CCAAT/enhancer binding protein-beta is a transcriptional regulator of peroxisome-proliferator-activated receptor-gamma coactivator-1alpha in the regenerating liver. Mol. Endocrinol. *22*, 1596–1605.

West, A.P., Brodsky, I.E., Rahner, C., Woo, D.K., Erdjument-Bromage, H., Tempst, P., Walsh, M.C., Choi, Y., Shadel, G.S., and Ghosh, S. (2011a). TLR signalling augments macrophage bactericidal activity through mitochondrial ROS. Nature *472*, 476–480.

West, A.P., Shadel, G.S., and Ghosh, S. (2011b). Mitochondria in innate immune responses. Nat. Rev. Immunol. *11*, 389–402.

Yang, C.T., Cambier, C.J., Davis, J.M., Hall, C.J., Crosier, P.S., and Ramakrishnan, L. (2012). Neutrophils exert protection in the early tuberculous granuloma by oxidative killing of mycobacteria phagocytosed from infected macrophages. Cell Host Microbe *12*, 301–312.